Available online at www.sciencedirect.com

SciVerse ScienceDirect

Ceramics International 38 (2012) 1879–1886

CERAMICS INTERNATIONAL

www.elsevier.com/locate/ceramint

Phase transformation during the sintering of γ-alumina and the simulated Ni-laden waste sludge

Yanchun Wang, Kaimin Shih *, Xiaobin Jiang

Department of Civil Engineering, The University of Hong Kong, Pokfulam Road, Hong Kong Special Administrative Region

Received 21 June 2011; received in revised form 4 October 2011; accepted 5 October 2011
Available online 12 October 2011

Abstract

This study investigated the fundamental phase transformation process when incorporating simulated nickel-laden waste sludge by alumina-based ceramic system. To match the required sintering conditions for commercial ceramic products as a development of waste-to-resource strategy, the investigation focused on the nickel incorporation behavior of γ-alumina in moderate to low temperature sintering environments (1250–750 °C) under a 3 h sintering process. X-ray diffraction (XRD) and Rietveld refinement were used to show the quantitative distribution of phases. The results demonstrated that γ-alumina interacted intensively with nickel oxide at sintering temperatures above 1000 °C. Furthermore, the densification effect of the sintering process is also illustrated, as this is crucial for developing the needed mechanical strength for practical applications. The findings in this study reveal that there is good potential for achieving the stabilization of nickel by thermal treatment with a γ-alumina containing precursor via moderate ceramic sintering temperatures.

Keywords: Rietveld refinement; Spinel; Densification; Ceramic sintering; Nickel sludge

1. Introduction

Among the major waste types, the treatment and disposal of waste containing hazardous metals, such as metal laden sludge and ash, remains a major challenge for the current waste treatment industry. Traditional waste disposal methods, such as landfills, are no longer acceptable in many regions of the world [1–3]. Even when solidified and encapsulated in cement based materials, metal-laden sludge still possesses enough long term metal leachability to be a cause of serious concern if discharged into the environment, because the main mechanism of metal immobilization was simply to reduce the surface area available for leaching. Consequently, the search for feasible strategies to replace the traditional disposal methods that can reliably stabilize the hazardous metal contained in waste and sustainably achieve the goal of putting it to beneficial use has been attracting increasing interest.

To further stabilize hazardous metals in waste solids, a large volume of studies have successfully demonstrated the use of thermal treatment to stabilize radioactive metals in either glass matrix (vitrification) or crystalline structures [4]. However, the high temperature required for vitrification, which is above the melting point of the silica or silicates in the system, not only consumes significant amounts of energy, but is also difficult to integrate into any of the existing industrial facilities. Ceramic materials encompass a wide variety of consumable, construction, and industrial products, such as tiles, bricks, and insulation and refractory products. The temperatures used to process ceramics can be much lower than for vitrification, for instance up to 800 °C for bricks and up to 1100 °C for tiles [5], and the metal-incorporated end products can still have the same functionality as originally designed for the marketable products. However, the fundamental metal incorporation process and phase transformation capability need to be investigated in detail to ensure a dependable and safe waste-to-resource technology. Further attempts to match the required sintering conditions to the equivalent processing parameters for commercial ceramic products would thus help to achieve the goal of being able to incorporate metals into existing production lines with very little, if any, additional cost.

Nickel is a major type of hazardous metal and nickel-laden sludge is discharged mainly as a result of industrial activity,

* Corresponding author. Tel.: +852 2859 1973; fax: +852 2559 5337.
E-mail address: kshih@hku.hk (K. Shih).

0272-8842/$36.00
doi:10.1016/j.ceramint.2011.10.015

especially in the electroplating industry. The wastewater and sludge generated from electroplating works usually contain high levels of nickel [6,7]. Nevertheless, the demand for these types of industrial practice is expected to continuingly increase [8]. Although it may be economically feasible to extract nickel from the waste streams for recycling purposes, this is usually limited to waste streams with high metal concentrations, and the residue from the recycling process still contains enough nickel to require proper pretreatment before it can be safely disposed. Experiments with simulated nickel-laden sludge have been carried out using lime to precipitate nickel from its nitrate and chloride solutions, or directly using nickel hydroxide [9,10]. Because nickel oxide is the final product of the aforementioned precursors in a high temperature environment, it should thus be the target compound for investigating incorporation when considering the stabilization of nickel-laden sludge. Previous studies have confirmed that a series of nickel spinel structures, such as $NiAl_2O_4$ and $NiFe_2O_4$, can be produced during the processes of sintering nickel oxide with alumina, hematite, kaolinite or mullite precursors [11–13]. Even though nickel oxide is scarcely soluble, the results derived from the leaching experiments strongly support the superiority of spinels in stabilizing nickel as they have significantly lower intrinsic metal leachability, when comparing to nickel oxide [12,13]. Therefore, a better understanding of the spinel formation mechanism and the rate of transformation, particularly in the lower temperature range, could effectively maximize the stabilization of nickel in the sintering processes for a wide range of ceramic products.

In a previous study, γ-alumina (γ-Al_2O_3) was found to have greater potential than α-alumina (α-Al_2O_3, corundum) for incorporating nickel at a low temperature range, i.e. between 1100 and 1160 °C [11]. However, the nickel incorporation capability of γ-alumina below this temperature range is still not clear. Accordingly, knowledge of this would be of great help in initiating an effective metal stabilization mechanism to apply to lower temperature ceramic products. This study thus focused on investigating the nickel incorporation behavior of γ-alumina at moderate to low temperature sintering environments (1250–750 °C). In addition, the study aimed to determine the quantitative incorporation efficiency at different sintering temperatures under a 3 h short sintering process. An X-ray diffraction (XRD) analysis with the LynxEye detector technique was used to obtain high quality diffraction data from samples under different thermal conditions, and the Rietveld refinement method was further adopted to quantitatively describe the distribution of crystalline phases in the system. Under the controlled nickel/aluminum mole ratio (1:2), the quantity of poor crystalline γ-alumina can also be resolved by the quantified crystalline phases. Furthermore, because the densification effect during the ceramic sintering process is crucial to the development of the mechanical strength of the final products, this study also observed the change of sample size under different sintering temperatures with the aim of identifying the sample densification progress. Although many other processing factors and material impurities may further influence the densification result of ceramic products, it is important to first understand the degree of such effect initiated by the nickel incorporation process. The findings of this study can be used to evaluate the potential of stabilizing nickel by γ-alumina containing precursor at temperatures lower than that of vitrification method and also explore the opportunities of reliably blending waste sludge into the manufacturing processes of marketable ceramic products.

2. Experimental methods

As the target compound for investigating incorporation, nickel oxide (NiO) was used to simulate nickel-laden sludge under thermal processing and was mixed with γ-alumina (γ-Al_2O_3) for the ceramic sintering experiment. The as-received NiO powder (Fisher Scientific) was confirmed by XRD for its mineral phase (Fig. A.1). The γ-Al_2O_3 was synthesized by heating HiQ-7223 boehmite (AlOOH; ICDD PDF 74-1895) powder (Alcoa Corp.) at 650 °C for 3 h (Fig. A.2). The successful conversion of boehmite to the γ-Al_2O_3 precursor was confirmed by the XRD patterns of γ-Al_2O_3 derived from other studies [14–16]. All the samples tested in the nickel incorporation experiment in this study were prepared by the solid-state sintering method. To obtain homogeneous raw material and controlled particle size, the mixtures of NiO and γ-Al_2O_3 powders were ball-milled for 22 h in a water-slurry form to obtain an average particle size at around 10 μm. The Ni/Al mole ratio of the raw material is 1:2, which is the stoichiometric maximum for nickel aluminate spinel ($NiAl_2O_4$). After ball milling, the slurry was dried at 95 °C for 3 days and homogenized again by mortar and pestle, before being pressed into 20 mm diameter pellets under 650 MPa pressure. The pelletized samples were then heated at a rate of 10 °C min^{-1} in a top hat furnace (Nabertherm) and sintered at temperatures between 750 and 1250 °C by a 3-h short sintering scheme to explore a more flexible application in ceramic industry [17,18]. The sintered samples were air-quenched, measured for change in diameter, and ground into powders for XRD analysis.

The X-ray powder diffraction data were collected on a D8 Advance Diffractometer (Bruker AXS) equipped with a Cu X-ray tube and a LynxEye detector operated at 40 kV and 40 mA. The system was calibrated by Standard Reference Material 660a (lanthanum hexaboride, LaB_6), obtained from the U.S. National Institute of Standard and Technology, for the line position. Scans were collected from 10° to 130° 2θ-angle, with a step width of $2\theta = 0.02°$ and a sampling time of 0.3 s per step. The X-ray diffraction data were processed by the FullProf Suite crystallographic program (version Feb-2007) for quantitative analysis of the phase compositions [19]. The FullProf Suite employs the Rietveld refinement method to match the observed diffraction pattern for determining the weight percentage of crystalline phases in a sample. To access the quality of matching results, the refinement analysis of each pattern generates the pattern factor (R_p), the weighted pattern factor (R_{wp}), the expected pattern factor (R_{exp}), and the goodness of fit (GOF) value defined by the following equations:

$$R_p = \frac{\sum |Y_{o,m} - Y_{c,m}|}{\sum Y_{o,m}} \quad (1)$$

$$R_{wp} = \sqrt{\frac{\sum w_m (Y_{o,m} - Y_{c,m})^2}{w_m {Y_{o,m}}^2}} \quad (2)$$

$$R_{\exp} = \sqrt{\frac{\sum M - P}{\sum w_m {Y_{o,m}}^2}} \quad (3)$$

$$\mathrm{GOF} = \chi^2 = \frac{R_{wp}}{R_{\exp}} = \sqrt{\frac{\sum w_m (Y_{o,m} - Y_{c,m})^2}{M - P}} \quad (4)$$

where $Y_{o,m}$ and $Y_{c,m}$ are the observed and calculated data, respectively, at data point m; M is the number of data points; P is the number of parameters; and w_m is the weighting given to data point m. The counting statistics is given by $w_m = 1/\delta(Y_{o,m})^2$, where $\delta(Y_{o,m})$ is the error in $Y_{o,m}$. The R_{wp}/R_{exp} ratio or the "goodness of fit (GOF)" value will be equal to one in an ideal refinement. However, in an actual situation, the background and peak profile mismatch lead to GOF > 1. A GOF value between 1.0 and 2.9 is generally considered satisfactory [20]. To further ensure the applicability and precision of the refinement method used for the phases shown in this study, a series of phase-mixture powder samples with known percentages of NiO, α-Al_2O_3, and $NiAl_2O_4$ spinel phases (ICDD PDF 77-1877) were refined by the FullProf Suite to obtain their quantitative phase compositions. The result comparison generally confirmed the good agreement between the compositions determined by refinement and the true compositions, as detailed in Table 1. The GOF values generated by these five refinement analyses, which were between 1.06 and 1.18, were also satisfactory. The Fig. B.1 further presents the match of experimental and calculated XRD patterns of these phase-mixture samples with known compositions.

3. Results and discussion

3.1. Formation of $NiAl_2O_4$ from γ-Al_2O_3 precursor

Pellet samples with a Ni/Al mole ratio of 1:2 were sintered at temperatures of 750, 850, 900, 950, 1000, 1050, 1100, 1150, 1200 and 1250 °C for 3 h as a test of the applicability of the short sintering process. The X-ray powder diffraction patterns of the sintered products are shown in Fig. 1. The position of the most intense diffraction peak of $NiAl_2O_4$ (at $2\theta = \sim 37.01^\circ$) was found to be strongly interred by the peak of NiO at $2\theta = \sim 37.25^\circ$.

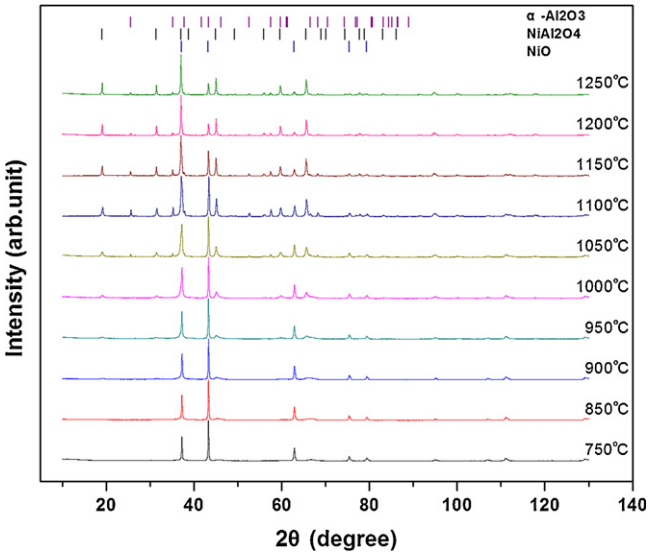

Fig. 1. X-ray powder diffraction patterns of NiO + γ-Al_2O_3 powder mixture samples sintered at different temperatures. The mixture had a NiO:γ-Al_2O_3 mole ratio of 1:1, and the sintering time was 3 h. The vertical bars on top of the patterns are expected Bragg positions of nickel oxide (NiO, $Fm-3m$), corundum (α-Al_2O_3, $R-3c$) and nickel aluminate spinel ($NiAl_2O_4$, $Fd-3m$).

Therefore, it is difficult to accurately identify the lowest sintering temperature for $NiAl_2O_4$ formation based solely on qualitative observations of its other diffraction peaks. The observable $NiAl_2O_4$ diffraction peaks in Fig. 1 indicate a possible range of 850–950 °C for initiating $NiAl_2O_4$ formation. Phillips et al. provided the first equilibrium phase diagram of the NiO–Al_2O_3 system and indicated the possibility of $NiAl_2O_4$ formation at thermal treatment above 1350 °C [21]. In 2006, Shih et al. reported the possibility of initiating $NiAl_2O_4$ formation at temperatures above 1000 °C using α-Al_2O_3 (corundum) as a precursor [11,12]. Nevertheless, this study used γ-Al_2O_3 as the precursor and the results suggest that an even lower temperature range can successfully initiate $NiAl_2O_4$ formation to stabilize hazardous nickel ions. The phase of γ-Al_2O_3 is a low-temperature polymorph of α-Al_2O_3 and has a defect spinel structure. The higher reactivity of γ-Al_2O_3 toward the incorporation of nickel into $NiAl_2O_4$ spinel phase may be thermodynamically realized due to the higher free energy of formation for γ-Al_2O_3, compared to that of α-Al_2O_3 [16]. When considering the formation of $NiAl_2O_4$ from the reaction between NiO and Al_2O_3, a higher free

Table 1
A precision test applying the Rietveld refinement method was used in this study to quantify the powder samples of the α-Al_2O_3, NiO, and $NiAl_2O_4$ phases. These compositional phases are the potential crystalline phases appearing in the sintered products, and the values generated to indicate the quality of fit results (R_p, R_{wp}, R_{exp} and GOF) are also provided.

Sample name	Compositions			Results of Rietveld refinement						
	α-Al_2O_3 (wt%)	NiO (wt%)	$NiAl_2O_4$ (wt%)	R_p (%)	R_{wp} (%)	R_{exp} (%)	GOF[b]	α-Al_2O_3 (wt%)	NiO (wt%)	$NiAl_2O_4$ (wt%)
S20NA40	40	40	20	2.90	3.72	3.16	1.18	42.1	37.4	20.5
S40NA30	30	30	40	2.72	3.42	3.23	1.06	33.2	28.1	38.7
S60NA20	20	20	60	2.68	3.36	3.11	1.08	21.7	19.0	59.3
S80NA10	10	10	80	2.78	3.50	3.13	1.12	10.5	9.9	79.6
S0[a]	57.7	42.3	0	2.93	3.70	3.37	1.10	59.0	40.4	0.6

[a] Mole ratio Al_2O_3:NiO = 1:1.
[b] Values between 1.0 and 2.9 to be satisfactory.

energy of formation for Al_2O_3 is energetically more favored. This may explain the initiation of $NiAl_2O_4$ formation at a lower temperature when using γ-Al_2O_3 as the precursor.

Under high temperature and with sufficient treatment time, γ-Al_2O_3 has been reported to transform to α-Al_2O_3, which has a hexagonal crystalline structure [14]. Under the sintering condition carried out in this study, the corundum phase was not observed in samples sintered at temperatures lower than 1050 °C, even though the remaining NiO reactant is clearly observable. This result further confirms that either γ-Al_2O_3 or α-Al_2O_3 can provide a reaction pathway for $NiAl_2O_4$ spinel formation (Eq. (5) or Eq. (6)):

$$NiO + \gamma\text{-}Al_2O_3 \rightarrow NiAl_2O_4 \quad (5)$$

$$NiO + \alpha\text{-}Al_2O_3 \rightarrow NiAl_2O_4 \quad (6)$$

Fig. 2 shows the temperature dependence of the peak intensity of the spinel phase and corundum, which manifests the change of the phase content. The peak intensity of the (1 1 1) reflection of $NiAl_2O_4$ in Fig. 2a shows the increase in spinel phase with the increase in sintering temperature. On the other hand, the content of corundum increased at a low temperature and achieves its maximum value at near 1100 °C, due to the more intensive spinel formation at higher temperatures. Such variation can be further observed from the peak intensity of the (0 1 2) reflection of corundum (Fig. 2b).

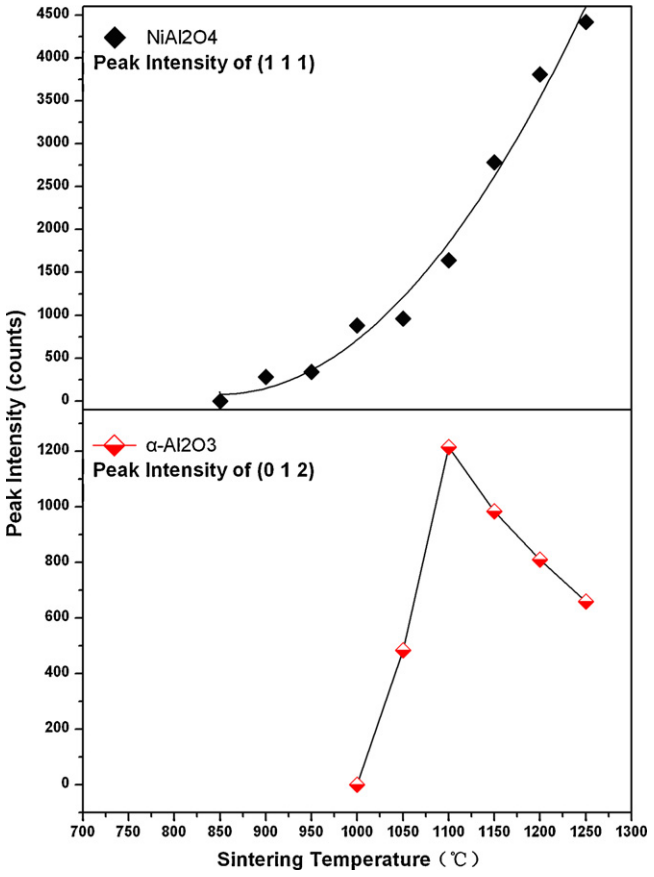

Fig. 2. The developed peak intensities of (a) $NiAl_2O_4$ spinel phase (1 1 1) reflection; and (b) α-Al_2O_3 (corundum) phase (0 1 2) reflection from NiO + γ-Al_2O_3 samples sintered at 850–1250 °C for 3 h.

3.2. Quantitative analysis of phase transformation

The Rietveld refinement technique was used to determine the relative weight percentages of the crystalline phases through the implementation on FullProf Suite. Typical refinement results successfully matching the calculated and experimental XRD patterns can be illustrated, as in Fig. B.2, which includes the analyses of samples sintered at 750, 1050 and 1250 °C for 3 h. The relative weight percentages of the crystalline phases (nickel oxide, corundum and spinel) for all sintering samples are provided in Table 2, which also includes the relevant fit parameters (R_p, R_{wp}, R_{exp} and GOF). As the GOF values obtained were generally between 1.23 and 1.41, the fitting quality is considered very satisfactory. As the Ni/Al mole ratio of the system was fixed at 1:2, the amount of the very poor-crystalline γ-Al_2O_3 can be calculated from the mass balance of the Al element and is also listed in Table 2 as the residual reactant.

Based on the XRD quantification results, a quantitative distribution for all phases (NiO, α-Al_2O_3, γ-Al_2O_3 and $NiAl_2O_4$) in the reaction system can be constructed as a function of sintering temperature (Fig. 3). To facilitate the delineation of phase transformation behavior, the reaction process can be classified into five stages (A–E) to illustrate the change trend of phases at corresponding temperature ranges. At stage A (<850 °C), no observable transformation of γ-Al_2O_3 to α-Al_2O_3 or to spinel phase was detected by the XRD measurement. Fig. B.2a shows a typical XRD pattern of the samples sintered at this stage, where only the peaks of NiO and the poor crystalline γ-Al_2O_3 were observed. At temperatures between 850 and 900 °C (stage B), the strong initiation of spinel crystallization effectively transformed NiO and γ-Al_2O_3 into the $NiAl_2O_4$ phase, presumably starting from the interface between the NiO and γ-Al_2O_3 particles. At stage C, the consumption of reactants and the increase in $NiAl_2O_4$ spinel products were both mitigated over the range of 900–1000 °C. Because the formation of $NiAl_2O_4$ from NiO and Al_2O_3 precursors requires the counter-diffusion of Ni and Al ions, the major factor of limiting the spinel growth at stage C is likely to be slower diffusion across the newly formed spinel barrier between its two oxide precursors.

Stage D features the appearance of corundum (α-Al_2O_3) and the further dramatic decrease of γ-Al_2O_3 in the system at temperatures between 1000 and 1100 °C. Samples sintered at this stage have overall higher crystallinity and a typical XRD pattern can be demonstrated, similar to that shown in Fig. B.2b. The appearance of α-Al_2O_3 indicated that the rate of structural change between the two alumina polymorphs (from γ to α type) was faster than the nickel incorporation rate by spinel phase at this stage. Observation of the NiO and $NiAl_2O_4$ quantities in the system shows the increasing trend of converting nickel from NiO to $NiAl_2O_4$ with elevated temperature was simply unaffected at this stage. When sintered at temperatures higher than 1100 °C (stage E), the poorly crystalline γ-Al_2O_3 was completely absent from the system. Although the rate of phase transformation from γ-Al_2O_3 to α-Al_2O_3 was still higher than that of $NiAl_2O_4$ spinel formation, the more intensive diffusion process due to the higher temperature still effectively converted nickel into the spinel structure. The final

Table 2
The results of the Rietveld refinement for quantifying the phase compositions of sintered products in Fig. 1. The values indicating the quality of fit (R_p, R_{wp}, R_{exp} and GOF) are also provided.

Sintering temperature (°C)	Results of Rietveld refinement							
	Quality of fitting				Compositions of sintered products (wt%)			
	R_p (%)	R_{wp} (%)	R_{exp} (%)	GOF[a]	NiO	α-Al_2O_3	$NiAl_2O_4$	γ-Al_2O_3[b]
750	3.80	4.87	3.71	1.32	42.3	–	–	57.7
850	3.89	4.91	3.73	1.32	42.3	–	–	57.7
900	3.07	3.90	3.15	1.24	27.1	–	35.9	37.0
950	3.88	4.93	3.75	1.31	24.0	–	43.2	32.8
1000	2.70	3.51	2.60	1.35	22.9	–	45.9	31.2
1050	4.07	5.36	3.79	1.41	21.1	13.3	50.1	15.6
1100	3.69	4.78	3.82	1.25	18.3	25.4	56.3	–
1150	3.85	4.98	3.95	1.26	16.1	21.1	62.8	–
1200	3.60	4.60	3.75	1.23	13.4	17.6	69.0	–
1250	3.79	4.85	3.79	1.28	10.8	13.2	76.1	–

[a] Values between 1.0 and 2.9 to be satisfactory.
[b] Calculated from the results of Rietveld refinement and the mass balance of Al content, which was maintained at the Ni/Al mole ratio of 1:2 in the system.

product sintered at this stage is highly crystalline, and a typical XRD pattern is shown in Fig. B.2c. At this stage, another major feature was the drastic decrease of α-Al_2O_3 in the system, which can also be realized due to its further participation in $NiAl_2O_4$ formation at higher temperatures (Eq. (6)).

Based on the results of the XRD quantitative analysis, a "transformation ratio (TR)" index can be used to indicate the efficiency of incorporating nickel into the $NiAl_2O_4$ spinel structure:

$$\mathrm{TR}\ (\%) = \frac{wt_{NiAl_2O_4}/MW_{NiAl_2O_4}}{wt_{NiAl_2O_4}/MW_{NiAl_2O_4} + wt_{NiO}/MW_{NiO}} \quad (7)$$

where *wt* is the weight percentage and *MW* is the molecular weight. For TR = 100%, complete transformation of nickel into $NiAl_2O_4$ structure is achieved; for TR = 0%, no nickel incorporation occurs. The $NiAl_2O_4$ curve in Fig. 3 can also reflect the TR values and directly indicates the efficiency of incorporating hazardous nickel into the more stabilized $NiAl_2O_4$ spinel structure [12]. The overall results of the quantitative analysis show the potential for significant nickel incorporation (>50%) into spinel structure in a moderate temperature sintering environment (1000 °C), even under a 3 h short sintering process. As the incorporation behavior showed a rapid increase in the transformation ratio at a lower temperature (stage B) followed by a steady increase with the increase in temperature (stages C–E), this suggests an intensive interaction between NiO and γ-Al_2O_3 and then, potentially, a diffusion-dominant process at higher temperatures. In contrast, in a previous study with α-Al_2O_3 as the precursor, the interaction with NiO was not able to be initiated before the temperature was increased to above 1000 °C [11].

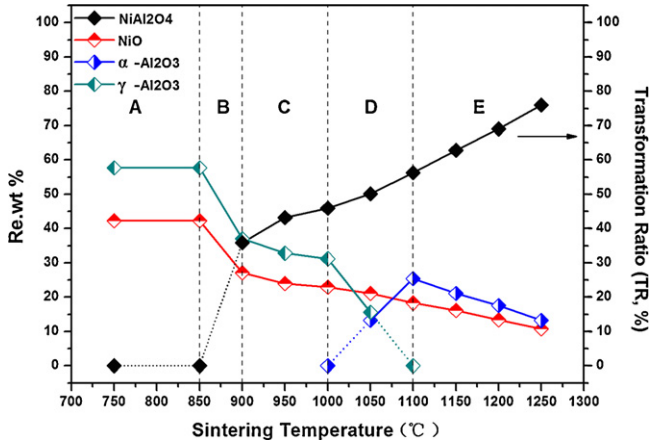

Fig. 3. Quantitative distribution of the compositional phases in the system of sintering NiO + γ-Al_2O_3 sample (Ni/Al mole ratio = 1:2) at temperatures between 750 °C and 1250 °C. The reaction process was classified into five stages (A–E) to illustrate the different behavior of the reacting phases within the sintering temperature ranges.

3.3. Thermal densification of ceramic products

In addition to the preferred chemical reactions between reactants, the densification effect after the sintering process can be quite beneficial in confining the stabilized product and eliminating the channels of potential chemical alteration, such as acidic leaching and weathering. In this study, because the raw materials were pressed into the same diameter (20 mm) pellets, the change in product pellet diameter can reflect the expansion or densification of the ceramic microstructure due to the 3 h sintering. It was found that the interaction between NiO and γ-Al_2O_3 led to a thermal densification effect (an inverse thermal expansion effect) – in the other words, all pellet diameters decreased after sintering (Fig. 4). However, significant densification was not achieved until the sintering temperature was higher than 900 °C, which was the lowest temperature of the stage C sintering. At stage B, the increase of sintering temperature showed the most significant increase in $NiAl_2O_4$ formation, although it did not produce much densification effect. Therefore, the formation of $NiAl_2O_4$ at this stage generally maintained the same microstructure as the raw material and is presumably dominated by the surface diffusion mechanism between grains during the sintering process.

At stage C, the diffusion and spinel reaction progressed more into the grains and started to result in the significant densification of the microstructure. This densification effect was found to be further intensified when the system was also

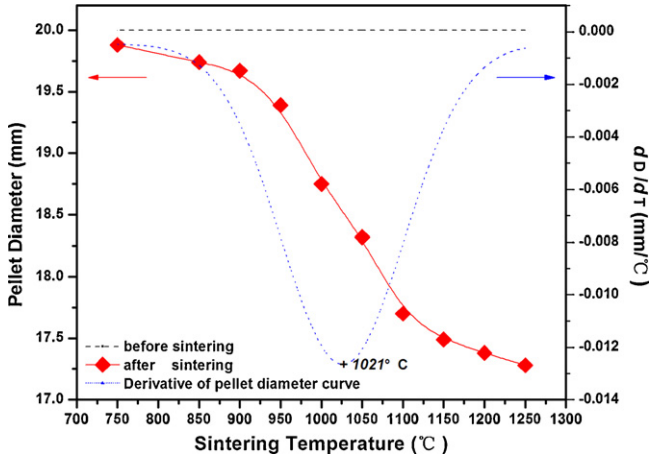

Fig. 4. Densification effect of sintering NiO + γ-Al_2O_3 pellets for 3 h. The initial (before sintering) pellet diameter was 20 mm. The derivative curve of product pellet diameter is also shown to indicate the effectiveness of enhancing densification at different temperatures.

accompanied by the polymorphic conversation of γ-Al_2O_3 to α-Al_2O_3 (stage D). γ-Al_2O_3 and α-Al_2O_3 are alumina polymorphs with noticeable differences in density. The density of γ-Al_2O_3 is 3.657 g cm^{-3} (ICDD PDF 79-1558) and that of α-Al_2O_3 is 3.983 g cm^{-3} (ICDD PDF 10-0425). Subsequently, the phase transformation from γ-Al_2O_3 to α-Al_2O_3 will further contribute to the densification of the sintered products and the smallest derivative was found to occur at stage D (∼1021 °C), which indicates the most efficient temperature range for enhancing the densification effect. After sintering at 1100 °C for 3 h, most of the densification effect has been achieved, to nearly 12% (with 2.3 mm shrinkage in pellet diameter). Further heating to 1250 °C only slightly increased the densification up to 14% (with 2.7 mm shrinkage in pellet diameter) in this study. In addition to the beneficial stabilization effects of densification, its potential influence on the product mechanical properties should also be an aid of this waste-to-resource strategy. The high metal incorporation efficiency and the densification effect delineated in this study have provided important information for minimizing the environmental impact of hazardous nickel sludge using the γ-Al_2O_3 ceramic precursor.

4. Conclusions

With the increasing demand for recycling waste materials in the interests of environmental sustainability, close attention is being paid to the development of new waste-to-resource technologies that minimize treatment costs and maximize the beneficial use potential of waste. The results of this study indicate that γ-alumina may have a key role as a precursor, particularly at sintering temperatures below 1100 °C, in stabilizing nickel-laden sludge so that it can be used in ceramic products. Compared to the use of α-alumina in previous study [11], both phase transformation and thermal densification data reveal that the γ-alumina precursor is capable of initiating the formation of nickel aluminate spinel and has a favorable densification effect at a temperature at least 100 °C lower in the 3-h sintering scheme. This finding suggests that there are new opportunities for incorporating nickel-laden sludge into a wide range of moderate temperature ceramic products when γ-alumina is part of the precursor material.

Acknowledgements

This work was financially supported by Hong Kong Research Grants Council (HKU 716310E, HKU 716809E) and University Grants Council (SEG_HKU10). The contribution of HiQ-7223 alumina by the Alcoa Corporation is gratefully acknowledged.

Appendix A. XRD patterns of raw materials

See Figs. A.1 and A.2.

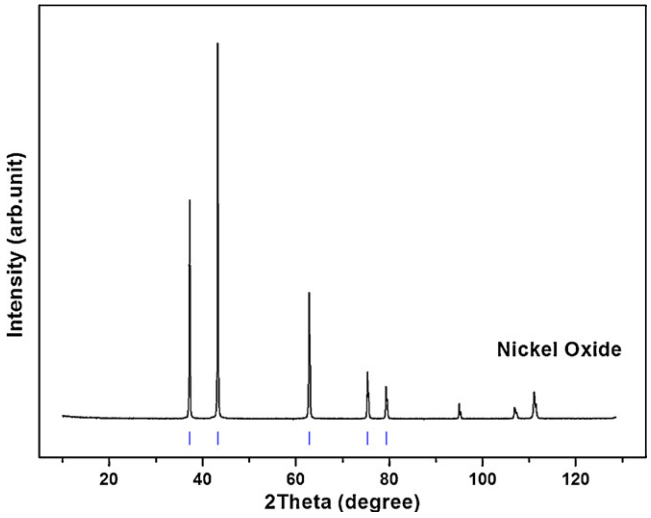

Fig. A.1. X-ray powder diffraction patterns of the nickel oxide raw material. The vertical bars at the bottom of the pattern are expected Bragg positions of nickel oxide (NiO; *Fm*−3*m*; ICDD PDF 78 0429).

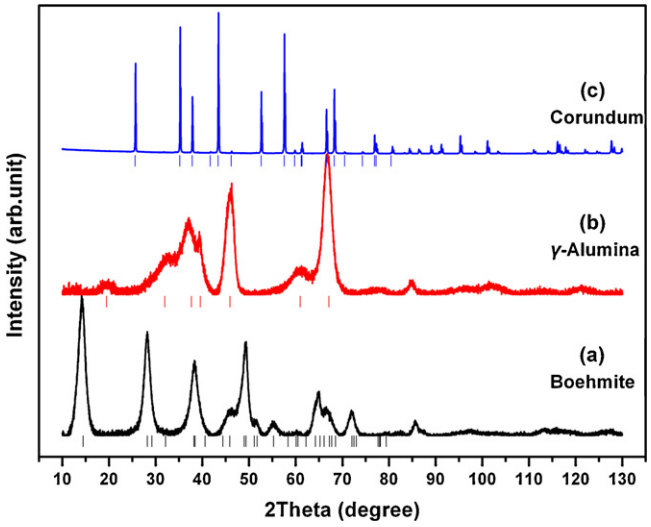

Fig. A.2. Mineral phases of the alumina precursors. XRD patterns of (a) HiQ®-7223 alumina powder; the Bragg positions represent boehmite (AlOOH; *Amam*; ICDD PDF 74 1895); (b) HiQ®-7223 alumina powder heated at 650 °C for 3 h; the Bragg positions represent γ-alumina (γ-Al_2O_3; *Fd*−3*m*; ICDD PDF 10-0425); (c) HiQ®-7223 alumina powder heated at 1500 °C for 6 h; the Bragg positions represent corundum (α-Al_2O_3; *R*−3*c*; ICDD PDF 83-2080).

Appendix B. Rietveld refinement results from the product XRD patterns

See Figs. B.1 and B.2.

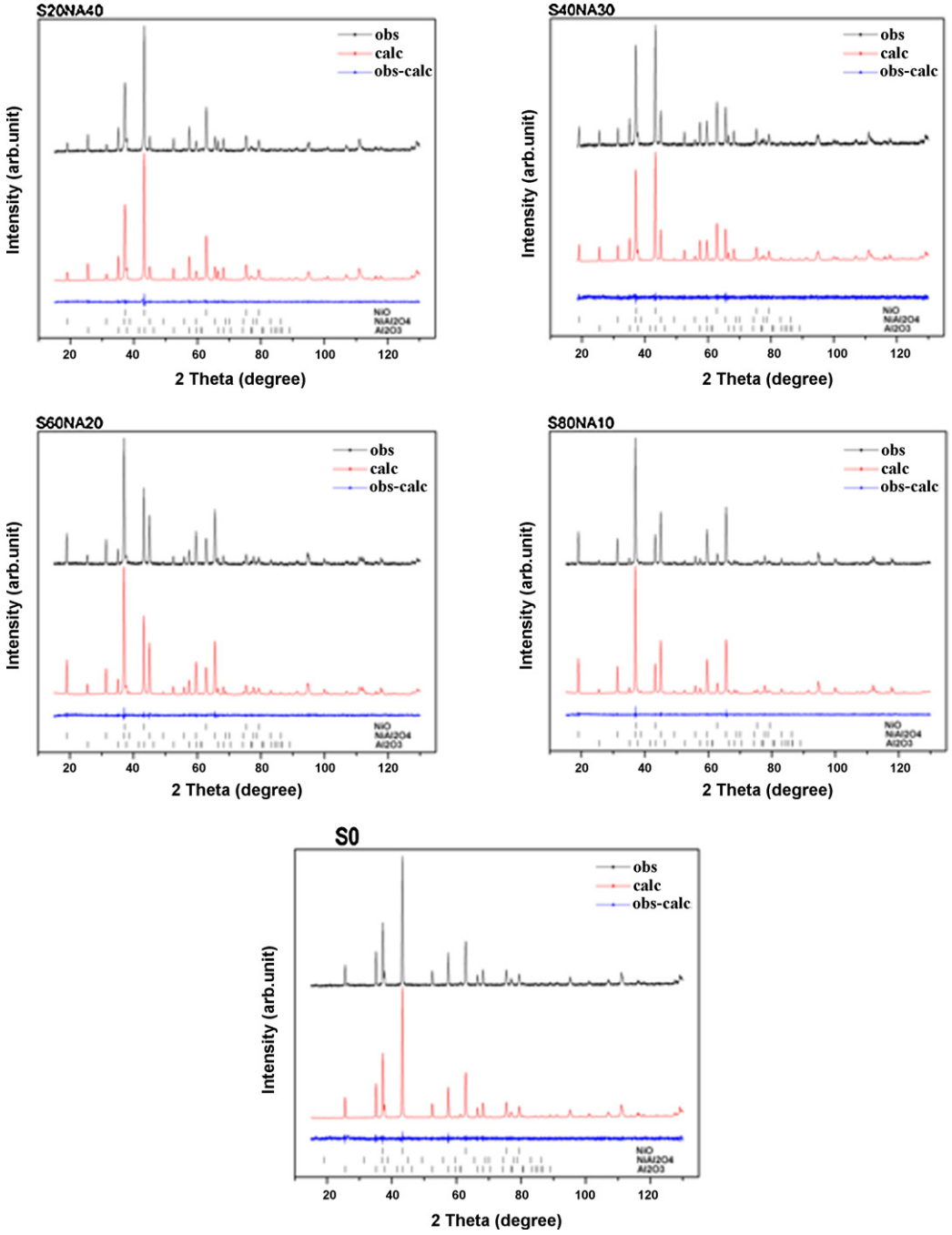

Fig. B.1. Experimental and calculated intensities of phase-mixture powder samples with known percentages of NiO, α-Al_2O_3, and $NiAl_2O_4$ spinel phases (Table 1). Differences between the experimental and calculated patterns are shown at the bottom of the figure. The vertical bars indicate the expected Bragg positions.

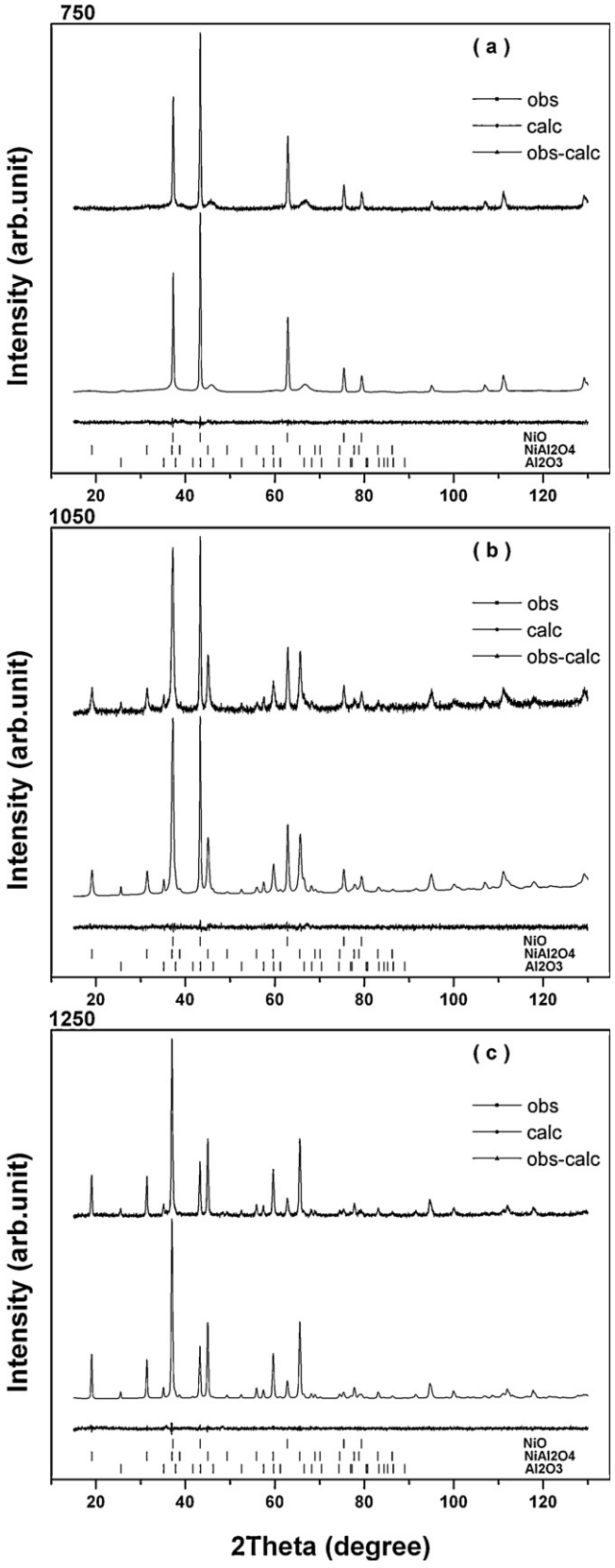

Fig. B.2. Experimental and calculated XRD patterns of sintered NiO + γ-Al_2O_3 samples (Ni/Al mole ratio of 1:2) at temperatures of (a) 750 °C, (b) 1050 °C, and (c) 1250 °C. The differences between the experimental and calculated patterns are shown as the bottom patterns in each figure. The vertical bars indicate the expected Bragg positions of potential crystalline phases in the system.

References

[1] V. Zania, P.N. Psarropoulos, Y. Karabatsos, Y. Tsompanakis, Inertial distress of waste landfills, Comput. Struct. 86 (2008) 642–651.

[2] D. Laner, J. Fellner, P.H. Brunner, Flooding of municipal solid waste landfills – an environmental hazard? Sci. Total Environ. 407 (2009) 3674–3680.

[3] D. Kulikowska, E. Klimiuk, The effect of landfill age on municipal leachate composition, Bioresource Technol. 99 (2008) 5981–5985.

[4] M.A. Lewis, D.F. Fischer, C.D. Murphy, Properties of glass-bonded zeolite monoliths, Ceram. Trans. 45 (1994) 277–286.

[5] A.R. Studart, U.T. Gonzenbach, E. Tervoort, L.J. Gauckler, Processing routes to macroporous ceramics: a review, J. Am. Ceram. Soc. 89 (2006) 1771–1789.

[6] P.T. Bolger, D.C. Szlag, Investigation into the rejuvenation of spent electroless nickel baths by electrodialysis, Environ. Sci. Technol. 36 (2002) 2273–2278.

[7] P.H. Chang, Y.H. Huang, C.L. Hsueh, M.C. Lu, G.H. Huang, Treatment of non-biodegradable wastewater by Electro-Fenton method, Water Sci. Technol. 49 (2004) 213–218.

[8] USEPA, Nickel Plating: Industry Practices Control Technologies and Environmental Management, USEPA Capsule Report 635/R-03/005, U.S. Government Printing Office, Washington, DC, 2003.

[9] A. Andres, R. Ibanez, I. Ortiz, J.A. Irabien, Experimental study of the waste binder anhydrite in the solidification/stabilization process of heavy metal sludges, J. Hazard. Mater. 57 (1998) 155–168.

[10] J.N. Diet, P. Moszkowicz, D. Sorrentino, Behaviour of ordinary portland cement during the stabilization/solidification of synthetic heavy metal sludge: Macroscopic and microscopic aspects, Waste Manage. 18 (1998) 17–24.

[11] K. Shih, T. White, J.O. Leckie, Spinel formation for stabilizing simulated nickel-laden sludge with aluminum-rich ceramic precursors, Environ. Sci. Technol. 40 (2006) 5077–5083.

[12] K. Shih, T. White, J.O. Leckie, Nickel stabilization efficiency of aluminate and ferrite spinels and their leaching behavior, Environ. Sci. Technol. 40 (2006) 5520–5526.

[13] K. Shih, J.O. Leckie, Nickel aluminate spinel formation during sintering of simulated Ni-laden sludge and kaolinite, J. Eur. Ceram. Soc. 27 (2007) 91–99.

[14] R.S. Zhou, R.L. Snyder, Structures and transformation mechanisms of η, γ and θ transition aluminas, Acta Crystallogr. B 47 (1991) 617–630.

[15] Y. Wang, C. Suryanarayana, L. An, Phase transformation in nanometer-sized γ-alumina by mechanical milling, J. Am. Ceram. Soc. 88 (2005) 780–783.

[16] C. Wolverton, K.C. Hass, Phase stability and structure of spinel based transition aluminas, Review B 63 (2000) 024102.

[17] D.D. Sun, J.H. Tay, H.K. Cheong, D.L.K. Leung, G.R. Qian, Recovery of heavy metals and stabilization of spent hydrotreating catalyst using a glass–ceramic matrix, J. Hazard. Mater. 87 (2001) 213–223.

[18] V.F. Pavlov, L.L. Alekseeva, V.S. Mitrokhin, Influence of the firing conditions upon the heat resistance of ceramic articles, Glass Ceram. 32 (1975) 674–676.

[19] J. Rodríguez-Carvajal, Recent advances in magnetic structure determination by neutron powder diffraction, Phys. B Condens. Matter. 192 (1993) 55–69.

[20] H. Fansuri, D.K. Zhang, D. French, M. Elcombe, A. Studer, An X-ray and neutron diffraction study of the structure of α-$Bi_2Mo_3O_{12}$ as a catalyst for partial oxidation of propylene to acrolein, in: Conference Proceedings. 32nd CHEMECA, Sydney, 2004.

[21] B. Phillips, J.J. Hutta, I. Warsaw, Phase equilibria in the system NiO–Al_2O_3–SiO_2, J. Am. Ceram. Soc. 46 (1963) 579–583.